http://dx.doi.org/10.5012/bkcs.2013.34.1.188

Aggregation of Laser-Generated Gold Nanoparticles Mediated by Formalin

Md. Alauddin, Kuk Ki Kim, Madhusudan Roy, Jae Kyu Song, Myung Soo Kim,† and Seung Min Park*

*Department of Chemistry and Research Center for New Nano Bio Fusion Technology, Kyung Hee University, Seoul 130-701, Korea. *E-mail: smpark@khu.ac.kr*
†Department of Chemistry, Seoul National University, Seoul 151-742, Korea
Received October 10, 2012, Accepted October 28, 2012

We have investigated the effects of formalin on the assembly of colloidal gold nanoparticles (AuNPs) prepared by laser ablation of a solid gold target in deionized water. Upon addition of formalin, the surface plasmon resonance (SPR) band at 519 nm for pure AuNPs decreases and shifts to red while a new broad SPR band appears at ~700 nm. The red-shift is prominent with increase in the incubation time. The average size of the initial AuNPs is around 12 nm but it increases to 23 nm after addition of formalin. It turns out that formalin acts as a cationic surfactant for AuNPs with negative surface charge in the colloidal solutions. Furthermore, through analysis of the Raman spectrum of formalin and the density functional theory calculations, we confirm that methanediol is the main species in formalin which is in charge of the aggregation of AuNPs.

Key Words : Gold nanoparticles, Formalin, Aggregation, Raman spectroscopy, Surface plasmon resonance

Introduction

Gold nanoparticles (AuNPs) have attracted great attention of researchers since they have extensive technological applications as well as unique properties.[1-10] When particles of gold are small enough, their color is ruby red due to strong absorption of green light at ~520 nm, the physical origin of which is the surface plasmon resonance (SPR): coherent oscillation of conduction band electrons induced by interacting electromagnetic field.[11-15] The SPR of noble metal nanoparticles is strongly dependent on the size, shape, interparticle interactions, dielectric properties, and local environment of the nanoparticles.[16]

As the size of nanoparticles is much smaller than the wavelength of incident light, energy can be confined in a small region through local excitation of the SPR. The intense electromagnetic fields around the nanoparticles are currently employed in a wide range of applications including optical energy transport,[17-19] chemical and biological sensors,[20-22] catalysis,[23-25] surface-enhanced Raman scattering (SERS),[26-30] near field scanning optical microscopy,[31] and nanoscale optical devices.[32,33] The electromagnetic field enhancement is spectacular when two or more metal nanoparticles are nearby; such positions, termed SERS "hot spots", can provide large enhancement factor (EF), which is crucial for the sensing or spectroscopic detection of molecules even at a single molecular level.

A simple system having such hot spots is achieved through aggregation of metal nanoparticles. Consequently, the assembly of nanoparticles is of paramount importance as SPR changes drastically depending on the interparticle spaces. In this regard, numerous experimental, theoretical, and computational studies have been performed to produce colloidal aggregation of nanoparticles over the past 30 years.[34-36] Also, various physical and chemical methods have been attempted to control the assembly of metal nanoparticles; aggregations through salting of citrate-capped colloids tend to showed poor control over size, gap, and topology, whereas organic monolayer-capped assemblies exhibited inconsistent and broad particle spacing.[37] On the other hand, rigid linking molecules such as DNA, biotin-streptavidin pairing, or multivalent thiols formed surface-functionalized nanoparticles which lead to separable aggregates.[38,39] Besides, thermal or pH response of capping materials on the nanoparticles has been also employed for reversible aggregations.[40-42] Despite the vast amount of works on nanoparticles aggregation, control over both particle spacing and the placement of molecules in the hot spots has not been successful. Also, aggregation mechanism and kinetic rates which determine the topology of the aggregates are still under investigation.

Very recently, a new technique has been developed by Nengsih *et al.* to detect formalin by comparing the localized surface plasmon resonance (LSPR) spectra of gold nanoparticles samples immersed in the deionized water and formalin (F) solution.[43] Formalin is an aqueous solution of formaldehyde. It typically contains 37 percent formaldehyde by weight and a small amount of stabilizer, usually 10 to 12 percent methanol. Formaldehyde reacts with water to form methanediol, which has a great abundance[44] in solution due to the following chemical reaction:

$$H_2C{=}O + H_2O \Leftrightarrow HOCH_2OH$$

Methanediol often leads to the formation of oligomers, depending upon the concentration of CH_2O, which is prevented with the help of methanol in solution. Formalin is widely used as a disinfectant or anti-bacterial agent.[45-49]

Nengsih *et al*. prepared gold nanoparticles on the quartz substrates using the seed mediated growth technique.[43] They reported that AuNPs with size of 35 nm were most effective to detect formalin. However, their work was limited just to

the detection of formalin without any analysis of the LSPR band shift in detail after addition of formalin in AuNPs solution. Here, we present experimental results on the kinetic evolution of different plasmon modes resulting from formalin-mediated assembly of AuNPs and the relationship between aggregated nanoparticles and the respective plasmon mode, which are evaluated by time-resolved optical excitation, Raman spectroscopy, zeta(ζ)-potential and dynamic light scattering (DLS) measurements. Also, we confirmed that methanediol is the main compound in formalin by taking Raman spectra of formalin. The interpretation of the Raman spectrum has been carried out through density functional theory (DFT) calculations with Gaussian 09W program package at B3LYP/cc-pVTZ level.

Experimental

AuNPs were prepared by laser ablation of a gold disk plate (99.99%) placed in a pyrex cell filled with 10 mL of deionized water. The gold target was irradiated for 20 min employing a Nd^{3+}-YAG laser (1064 nm, 10 Hz, Continuum, Surelite II) with pulse energy of 100 mJ. The laser beam was tightly focused using a lens with a focal length of 250 mm and the spot size of the focused laser beam was ~1.0 mm in diameter. The cell was continuously rotated to minimize the target aging effect and to give some stirring effect during the formation of gold nanoparticles. The concentration of AuNPs in the solution so produced was estimated to be 1.8×10^{-8} M after 12000 laser shots.

Aggregation of AuNPs was initiated upon addition of formalin (Sigma-Aldrich, 37 wt % in water, 12.32 M) to a colloidal solution of AuNPs (1.8×10^{-8} M). Chemisorption of methanediol molecules in formalin on the AuNPs surfaces by formation of Au-O···H bonds initiated aggregation. A series of mixed solutions with various concentration ratios (AuNPs:F = 10:1, AuNPs:F = 10:5, AuNPs:F = 10:7 by volume) were prepared to locate the optimal condition for producing AuNPs aggregates which were high stable over 6 h of incubation time without precipitation. To prepare a mixed solution with AuNPs:F = 10:1, for example, 1 mL (12.32 M) of formalin was added to 10 mL of AuNPs colloidal solution (1.8×10^{-8} M).

AuNPs were characterized using transmission electron microscope (TEM, Tecnai, G2 F30), UV-visible spectroscope (Shimadzu, UV-1800), dynamic light scattering equipment (DLS, K-ONE, Scatteroscope-I), and electrophoretic light scattering spectroscope (Otsuka Electronics, ELS-8000). To evaluate ζ-potentials of AuNPs, the mobility of the colloidal particles was measured by electrophoresis and ζ-potentials were calculated from the electrophoretic mobilities by Henry's equation. A 5 mm quartz cell was used for all the measurements of UV-visible spectra. TEM samples were prepared by dropping the AuNPs colloidal solution on a carbon-copper grid (Ted Pella, 400 mesh) followed by a drying process at room temperature. Dropping started 50 min after preparation of AuNPs colloidal solutions. Raman spectrum of formalin was obtained by employing a home-built micro-Raman spectrometer. Formalin was taken in a capillary-tube and spectrum was acquired with 532 nm He-Ne laser of 50 mW.

Results and Discussion

Raman Identification of Formalin. To establish the mechanism of the reaction of formalin with gold nanoparticles, it is essential to identify the main compound in formalin; we have taken Raman spectrum of formalin in the region of 250-4000 cm^{-1} which is shown in Figure 1(a). Identification of the Raman bands was carried out through density functional theory calculation. Figures 1(b) and 1(c) show the calculated Raman spectra for methanediol and formaldehyde, respectively. It is of note that the positions and number of Raman bands observed are coincident with those calculated for methanediol while those for formaldehyde are far away from the experimental Raman bands.

In more detail, the band observed at 567 cm^{-1} in Figure 1(a) was assigned to the δ(OCO) torsional vibrational mode of methanediol, $HOCH_2OH$.[50] The next intense band at 921 cm^{-1} was assigned to the symmetric C-OH stretching mode. The next three intense bands along with three weak bands observed at 1058, 1263, 1487, 1125, 1319, and 1421 cm^{-1} which were assigned as -CH_2 rocking, -CH_2 twisting, -CH_2 scissoring, -OH rocking, -OH scissoring, and -CH_2 wagging modes, respectively. The positions and relative intensities of these bands are closely coincident with those calculated for structure **I** (methanediol) shown in Figure 1(b). The assignments of the observed and calculated Raman bands for

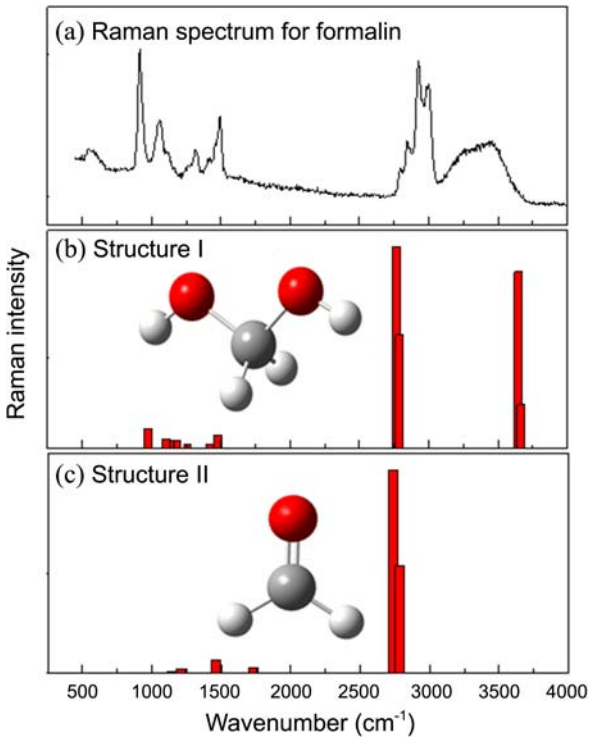

Figure 1. (a) Raman spectrum of formalin in the region of 250-4000 cm^{-1} and DFT-calculated spectrum of methanediol (b) and formaldehyde (c).

Table 1. Observed and calculated Raman band positions for methanediol in formalin

Observed frequency/cm^{-1}	Calculated frequency/cm^{-1}	Assignments
567	–	–
921	975	C-OH symmetric stretching
1058	1104	-CH_2 rocking
1125	1158	-OH rocking
1263	1194	-CH_2 twisting
1319	1259	-OH scissoring
1421	1423	-CH_2 wagging
1487	1478	-CH_2 scissoring
2797	–	Non-fundamental band
2847	–	Non-fundamental band
2929	2768	-CH_2 symmetric stretching
2994	2786	-CH_2 symmetric stretching
3313	3646	-OH asymmetric stretching
3441	3666	-OH asymmetric stretching

Calculated using B3LYP/cc-pVTZ Level of theory. Calculated values were corrected by multiplying the frequency factor, $f = 0.950$

methanediol are listed in Table 1. The two most intense bands observed at 2929 and 2994 cm^{-1} were assigned to the symmetric and anti-symmetric stretching modes of CH_2 group,

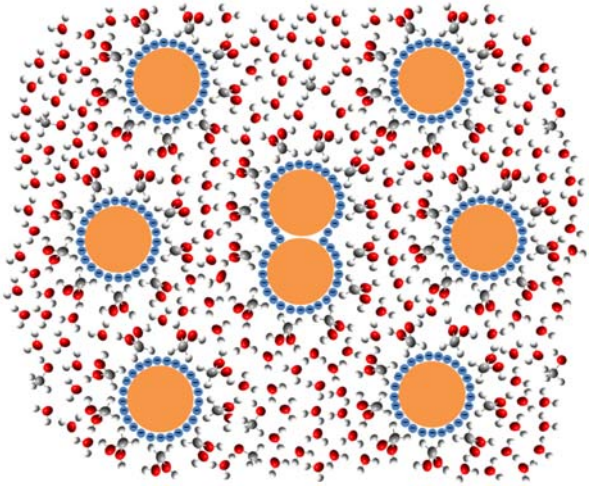

Figure 2. Assembly of gold nanoparticles (AuNPs) in formalin.

respectively. The two bands at 2797 and 2848 cm^{-1} are not assigned by the calculated spectrum. Mohlmann found that the depolarization ratios of the bands located at 2803 cm^{-1} and 2844 cm^{-1} are identical with that measured for the symmetric CH_2 mode at 2917 cm^{-1}.[51] These two lower wavenumber bands are generally considered to be the non-fundamental modes. The band observed at 3313 and 3441 cm^{-1}

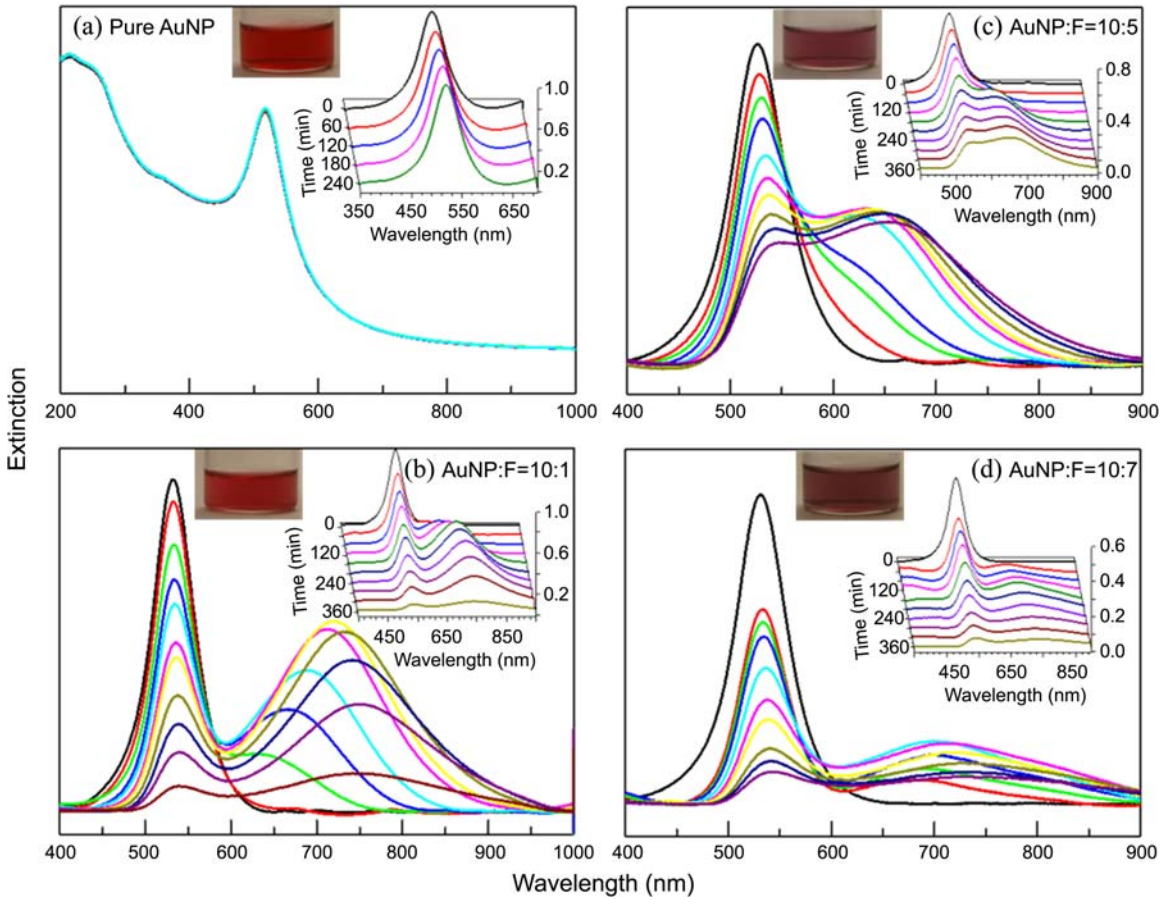

Figure 3. Time-resolved extinction spectra of (a) pure gold nanoparticles (AuNPs), (b) AuNPs:F (10:1), (c) AuNPs:F (10:5) and (d) AuNPs:F (10:7). Spectra were acquired at 20 min intervals for 3 h. The inset shows three dimensional optical absorption spectra and color of the AuNPs for the respective ratios.

were assigned to the symmetric and anti-symmetric stretching modes of -OH group of methanediol, respectively. On the other hand, Raman calculated spectrum of formaldehyde shows six bands at 1142, 1205, 1459, 1732, 2733, and 2784 cm^{-1} which were assigned as $-CH_2$ wagging, $-CH_2$ rocking, $-CH_2$ scissoring, C=O stretching, symmetric, and anti-symmetric stretching modes of CH_2 group, respectively. We have not observed any C=O stretching vibration in our experimental Raman spectrum but we observed just symmetric and *anti*-symmetric OH stretching vibrations, which strongly supports our calculated spectrum for methanediol. From these evidences, it is clear that methanediol is the main compound in formalin.

Time-Resolved Extinction Spectra of AuNPs and AuNPs:F Solutions. A schematic of AuNPs in formalin solution is depicted in Figure 2; parts of the AuNP surfaces are coated with methanediol molecules, which are surrounded by water molecules. The $-CH_2$ groups of methanediol molecules are positioned to face AuNPs due to the negative charge on AuNPs. In order to understand the effects of methanediol on the plasmonic characteristics of AuNPs, we examined the change in the extinction spectra, in a time-resolved manner, at various concentrations of formalin; Figure 3 presents a time-evolution of UV-visible spectra of (a) pure AuNPs, (b) AuNPs:F (10:1), (c) AuNPs:F (10:5), and (d) AuNPs:F (10:7) solutions. In Figures 3(b)-(d), the extinction spectra were base-line corrected to extract the main and secondary SPR band more clearly. Extinction spectra were acquired for pure AuNPs solution for 4 h at 1 h intervals while, in case of AuNPs:F solutions, they were measured for 6 h at 40 min intervals. The insets of Figure 3 display three dimensional extinction spectra together with photographs of each solution. The extinction spectrum of pure AuNPs solution exhibits an intense SPR band with a peak at 519 nm (Figure 3(a)) and the broad band extending toward the UV region is ascribed to the interband transition.[52] We have not observed any significant change in the peak position and intensity with increase in the incubation time (over 4 h) in case of pure AuNPs solution. This indicates that laser-generated AuNPs solution is highly stable and the shape of AuNPs is mostly spheroidal.

It is well known that the peak position and intensity of SPR band strongly depend on the diameter of NPs and the dielectric property of the medium.[13] Figure 4 shows the TEM images of (a) pure AuNPs, (b) AuNPs:F (10:1), (c) AuNPs:F (10:5), and (d) AuNPs:F (10:7) together with size distributions. For pure AuNPs, the average size of AuNPs was 11.7 nm in diameter and some aggregates were detected in the TEM image. In the laser fluence employed in our experiment, NPs are expected to be generated from explosive ejection of molten droplets as well as thermal vaporization.[53] However, it is not clear whether the aggregates were formed during the drying process for sample preparation or they were already contained in the colloids.

As we add formalin into the AuNPs solution to give AuNPs:F=10:1, the main SPR band decreased and red-shifted gradually, while a new broad SPR band grew and its peak shifted to red with time as shown in Figure 3(b). After ~3 h, the second SPR band intensity began to decrease. The intensity of the main SPR band position was initially 532 nm, shifted to red by 13 nm compared to pure AuNPs. This shift stems mainly from the following two factors induced by addition of formalin: the change in the dielectric properties of the layer around AuNPs and the increases in the aspect ratio of AuNPs via dimer formation.[54-59] Over 6 h, the SPR peak shifted slowly to 541 nm, which reflects further aggregation of AuNPs.

The optical absorption coefficient of nanoparticles with diameters smaller than the incident wavelength is determined by Mie theory, where the dielectric function is written as a combination of interband and intraband term (a Drude term).[60] Mie theory is a mathematical-physical description of the scattering of electromagnetic radiation by spheroidal particles immersed in a continuous medium.[61] When the shape of the nanoparticles deviates from the sphericity, Mie theory is no longer applicable. In this respect, Gans modified Mie theory which is now known as Mie-Gans theory[62] for metal NPs whose structural symmetries are away from

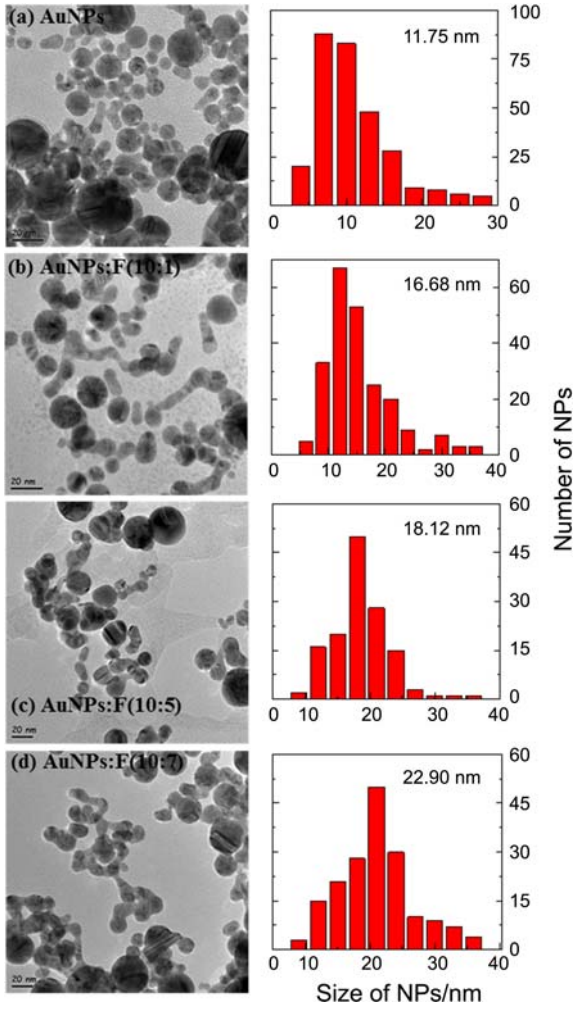

Figure 4. TEM images of (a) pure gold nanoparticles (AuNPs), (b) aggregation products for AuNP:F = 10:1, (c) aggregation products for AuNPs:F = 10:5, (d) aggregation products for AuNPs:F = 10:7. The size distributions of nanoparticles are shown on the right.

sphericity and predicted that a shift in SPR occurs when the particles deviate from the spheroidal geometry.

According to Gans, plasmon absorption splits into two bands for gold nanorods;[63] one, corresponding to the oscillation of the free electrons along the long axis and the other, perpendicular to the axis. The transverse mode shows a resonance at ~520 nm for AuNPs, which is co-incident with the plasmon band of spheroidal particles while the resonance of the longitudinal mode is red-shifted and strongly depends on the aspect ratio. In Figure 3(b), the main SPR band at 532 nm and the second SPR band at 725 nm correspond to the transverse and longitudinal mode, respectively. The SPR band for pure AuNPs exhibits at 519 nm while it shifted to 532 nm after addition of formalin; the considerable shift of the main SPR band, from 519 to 532 nm, is ascribed to the changes in the dielectric properties of the surrounding layer of AuNPs as well as the aspect ratios.[54-59] In the TEM image for AuNPs from AuNPs:F = 10:1 solution shown in Figure 4(b), we can clearly see the deviation of AuNPs from its sphericity as they aggregate and the average size of AuNPs is 16.6 nm.

In case of AuNPs:F = 10:5, the main SPR band is located at 526 nm which shifted to 543 nm over 6 h of incubation time. With increase in the incubation time, a secondary broad SPR band due to aggregation appeared and its peak maximum shifted to a maximum of 650 nm shown in Figure 3(c). The intensity of the second SPR band decreased slowly for AuNPs:F = 10:5 solution compare to AuNPs:F = 10:1. Figure 4(c) shows the TEM image for AuNPs from AuNPs:F = 10:5 solution and their size distribution, where the average size of AuNPs is slightly larger and the chain length was shorter compared to AuNPs from AuNPs:F = 10:1; the aver-

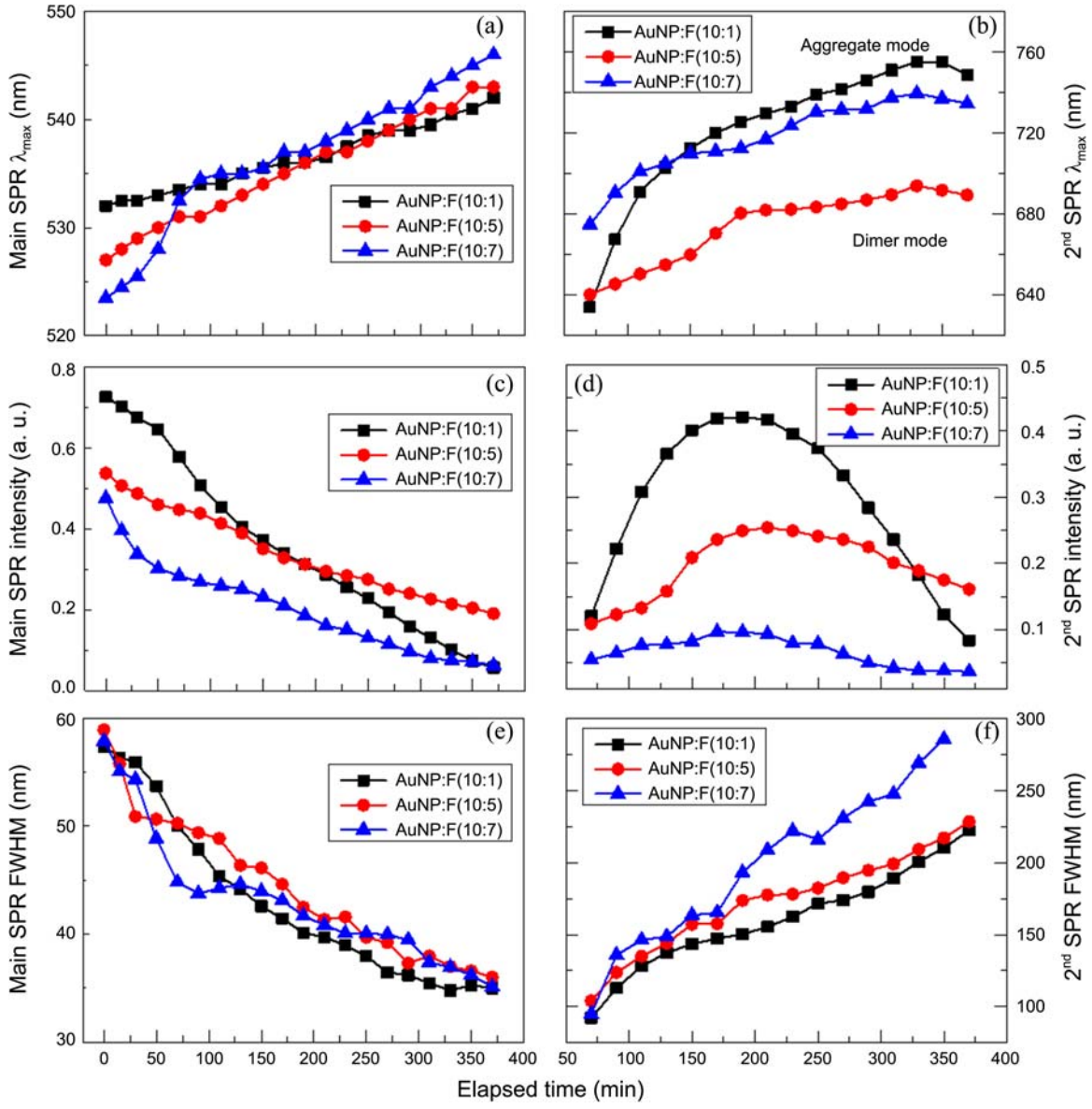

Figure 5. (a-b) The maximum wavelength of the main and the 2nd surface plasmon resonance (SPR λ_{max}) of gold nanoparticles (AuNPs), (c-d) The intensity of the main and the 2nd surface plasmon resonance band of AuNPs, and (e-f) FWHM of the main and the 2nd surface plasmon resonance of AuNPs at three different formalin ratios. The spectra were acquired at 20 min intervals for 6 h.

age size was 18.1 nm from the TEM image.

For AuNPs:F = 10:7, the main SPR band decreased rapidly with increase in the incubation time and the secondary SPR band was very weak as shown in Figure 3(d). Right after addition of formalin, the position of main SPR band was 531 nm, which shifted to red and its intensity decreased rapidly with time. After 6 h, the intensities of both bands decreased significantly due to formation of huge clusters by cross-linking aggregation of AuNPs. Figure 4(d) shows the TEM image for AuNPs from AuNPs:F = 10:7 which manifests prevailing cross-linkings of AuNPs. The average size of AuNPs was 22.9 nm.

The Aggregation Mechanisms: The Effects of Formalin Concentration.

Time-Evolution of the Extinction Spectra: Changes in the position of the peak maxima, peak intensity, full width half maximum (FWHM) for the main and secondary SPR band as a function of the incubation time at three different AuNPs:F ratios are collected in Figure 5. For AuNPs:F = 10:1 ratio, the maximum wavelength for main SPR band was 532 nm right after addition of formalin. Over 6 h of incubation time, it shifted to red up to 542 nm and the intensity decreased, which indicates that AuNPs were aggregated to give non-spheroidal geometry due to formation of dimers.

When formalin solution was added, the aggregation of AuNPs was not apparent up to ~50 min without any bonded network. After 50 min, we observed that a broad secondary SPR band appeared at ~660 nm, which reflects the aggregation of AuNPs. Over time, the intensity of this band increased to reach a maximum at 725 nm and again decreased to show its peak at 760 nm; in more detail, with addition of formalin, the repulsion between AuNPs becomes reduced due to the chemisorption of methanediol molecules on the surface of AuNPs, which helps two neighboring AuNPs form a dimer and the density of dimers so produced increases with time to result in the peak maximum at 725 nm after 200 min. After all, trimers, tetramers, and chain networks are also formed with increase in the incubation time and the secondary SPR band shifted further from 725 nm with its intensity decreased. Ultimately, the intensities of both SPR bands nearly vanished as AuNPs were denatured forming long chain networks mediated by methanediol molecules.

Through analyses of the time-dependent changes in the peak intensities and positions of the main and secondary SPR band, we can extract information on kinetics relevant to aggregation of AuNPs triggered by addition of formalin. Among three different AuNPs:F ratios, AuNP dimers seem to be less stable in case of AuNPs:F = 10:1 and AuNPs:F = 10:7 compared to AuNPs:F = 10:5. When the concentration of formalin is dilute in the solution such as AuNPs:F = 10:1, dimers of AuNP are formed faster, which is clear from the rapid growth of the peak intensity of the secondary SPR band as depicted in Figure 5(d), because the van der Waals interaction overwhelms electrostatic repulsion at low concentration of formalin. The formation of chain networks becomes accelerated as the density of the dimers or oligomers increases in the solution. However, it is possible at the expense of the dimers or oligomers which contribute to the secondary SPR band. When the concentration of formalin is extremely high (AuNPs:F = 10:7), the growth of the secondary band is not quite prominent although the depletion rate of the main band is noticeable as shown in Figures 5(c) and (d). Hence, this type of kinetic growth mode can be termed as "aggregate mode",[64] where dimers or oligomers turn into large aggregates, or chain networks, rapidly upon addition of formalin.

On the other hand, for medium concentration of formalin (AuNPs:F = 10:5), the main SPR band at 526 nm decreased most smoothly over the 6 h of incubation time and both the growth and decay rate of the secondary SPR band were medium values. The stability of AuNPs in this solution is inferred from the followings: the peak position of the secondary SPR band was around 660 nm while it was 725 nm and 710 nm, for 10:1 and 10:7 ratio, respectively and the decay rate of its intensity was slow, which is indicative of the prolonged lifetime of the dimers or oligomers. Namely, the van der Waals interaction, the Brownian motion, and electrostatic repulsion between AuNPs are well balanced at 10:5 ratio to guarantee longer time stability of AuNP dimers and oligomers; this kinetic growth mode is called "dimer mode".[64] Formation of dimers, oligomers, and chain networks at various AuNPs:F ratios is apparent as displayed in the TEM images of Figure 4.

We also measured the intensities of the main and the secondary SPR bands; the main SPR band, in all ratios, smoothly decreased with increase in the incubation time while the time-dependences of the secondary SPR bands were not monotonous as shown in Figures 5(c) and 5(d), respectively. The increase in the secondary SPR band in earlier times (up to ~175 min), as in the case of AuNPs:F = 10:0.1 as depicted in Figure 5(d), represents the formation of dimers and oligomers which can contribute to the intensity of the secondary SPR band. As the incubation time passes ~175 min, consecutive aggregations give birth to larger chain structures, which can no longer contribute to the secondary SPR band. We also evaluated the FWHMs of the main and the secondary SPR band; after base-line correction, both SPR bands were fit to Lorentzian, assuming symmetric plasmon band.[65] Figures 5(e) and 5(f) show different time-evolutions in the FWHMs of the main and the secondary SPR band for three different AuNPs:F ratios; the FWHM decreased with time for the main SPR band while it increased for the secondary due to aggregations.

Analysis of the Dynamic Light Scattering Data. Figure 6 shows the average size of AuNPs provided by DLS measurements, as a time-resolved manner, for different concentrations of AuNPs:F ratios. In case of pure AuNPs, size of NPs was around 11.7 nm by TEM image as shown in Figure 4(a) while it was 13.6 nm by DLS measurements. The discrepancy between the two is, of course, reasonable because hydrodynamic diameters are given by DLS. (The results on particle sizes determined by DLS and TEM may differ because of the solvent. In DLS, samples are fully solvated and swollen

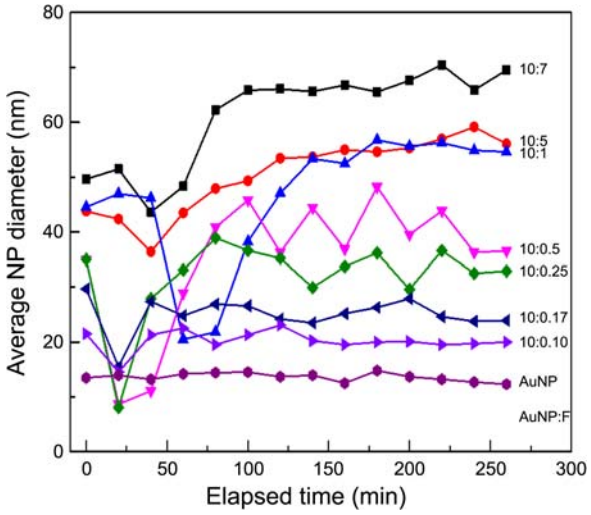

Figure 6. Time-resolved hydrodynamic diameter of gold nanoparticles (AuNPs) at different formalin concentrations.

while they are desolvated through drying process as probed by TEM. Another reason for the differences is the counting method; spheroidal particles were counted in TEM but each dimer, trimer, or large aggregate was counted as single particle

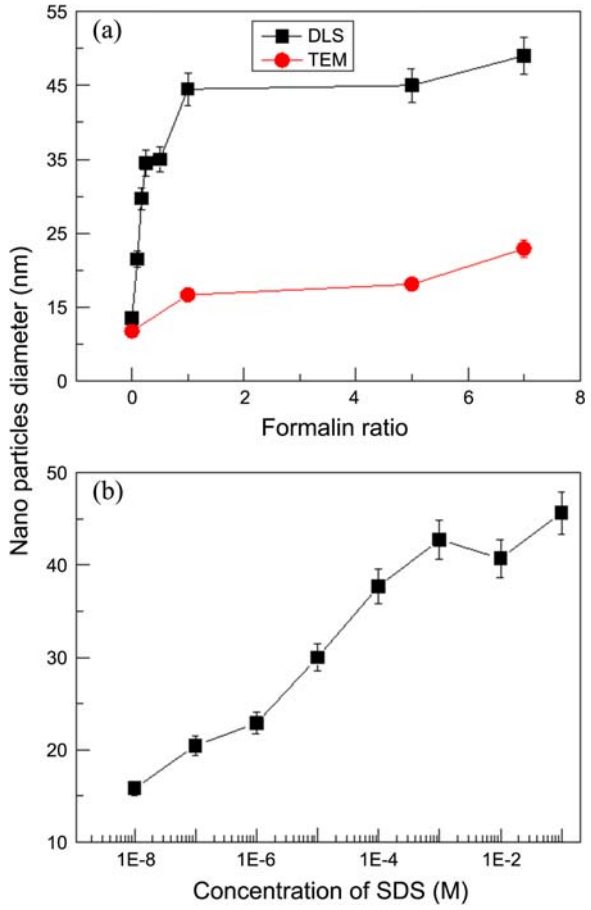

Figure 7. The size of nanoparticles (a) at different formalin ratios and (b) at different sodium dodecylsulfate (SDS) concentration, right after preparation of the solution.

in DLS.) However, as we added formalin in the colloidal solution of AuNPs, the average sizes of NPs were far off from those obtained by TEM images; the average sizes of AuNPs in 10:1, 10:5, and 10:7 ratios were 16.7, 18.1, and 22.9 nm, respectively, by TEM, while they were 40, 46, and 60 nm by DLS. When we reduced the ratio down to 10:0.1, the difference in the size measurements by TEM and DLS was not so pronounced as shown in Figure 7(a).

To verify the role of formalin in AuNPs solution, we have also adopted an anionic surfactant, sodium dodecylsulfate (SDS). SDS proved to be a good stabilizer, with which NPs were stable up to six months.[66] Figures 7(a) and (b) show the average sizes of AuNPs right after addition of different concentrations of formalin and SDS, respectively, as measured by DLS. In case of SDS, 5 mL of SDS solution was mixed with 10 mL of AuNPs solution. With increase in the concentration of SDS solution from 10^{-8} to 0.1 M, the size of AuNPs increased from 15 to 45 nm as shown in Figure 7(b), which is similar to the case of formalin. This certainly implies that the aggregation of AuNPs does not necessarily occur right after addition of formalin.

Figure 6 displays the time evolution of the average size of AuNPs as measured by DLS; upon addition of formalin, it increases rapidly far beyond that of the pure AuNPs solution, decreases after some time depending upon the AuNPs:F ratio, and then increases gradually up to the initial size (low formalin ratios) or larger size (high formalin ratios). Methanediol molecules in formalin can neutralize the negative charge on AuNPs by chemisorption of -CH_2 group of methanediol and thus the repulsion with AuNPs is reduced to promote the aggregation of AuNPs. Therefore, the initial size of AuNPs after addition of formalin increases with the AuNPs:F ratio as shown in Figure 6. After the initial increase, the average size drops down rapidly even below that of pure AuNPs due to the depletion of large aggregates which contribute to the formation of large precipitates. As time goes on, unstable small AuNPs aggregate and AuNPs resume its initial size and grow even further before they are stabilized. Methanediol molecule, $HOCH_2OH$ may react with each other and form long chain structures, which in turn play certain role to make AuNPs stay apart.[67]

The Effects of Formalin on the ζ-Potential. Despite the absence of stabilizers, noble metal nanoparticles produced by laser ablation in liquid (LAL) in various media including deionized and organic solvents are anomalously stable for days and even up to several months.[68-70] We also confirmed that AuNPs prepared by LAL in deionized water are stable after one month without any stabilizing agents. The surfactant-free AuNPs so produced are inherently stable mainly because their surfaces are negatively charged.

Sacher and co-workers[71] prepared gold nanoparticles by laser ablation in water using femtosecond pulsed laser and proved that the gold atoms on the nanoparticle surface are partially oxidized to Au-OH or $Au\text{-}O^-$ with an equilibrium between Au-OH or $Au\text{-}O^-$:

$$Au\text{-}OH \leftrightarrow Au\text{-}O^- + H^+$$

Table 2. Particle size distributions and zeta-potential values for different concentration ratios of AuNPs:F

Nonoparticles solution	Size distribution (nm)	Mean particle size (nm)	Zeta-potential (mV)
Deionized water	1-40	11.75	−39.94
AuNPs:F = 10:1	1-40	16.68	−11.46
AuNPs:F = 10:5	1-40	18.12	+0.30
AuNPs:F = 10:7	1-40	22.90	–

where the equilibrium shifts depending on the pH of the solution. By ζ-potential measurements, they found that oxygen atoms are negatively charged as Au-O^- at pH > 5.8 while they are reduced as Au-OH at pH < 5.8. Mafune and co-workers estimated that about 3-7% of the surface gold atoms owned a negative charge by titration with cationic surfactant like cethyltrimethyl ammonium bromide (CTAB).[67] Koshizaki *et al.* reported that the pH of the NPs solution was nearly unchanged after laser ablation, which confirmed the results of Mafune and coworkers that only a low percentage of surface atoms are oxidized.[53]

In our experiment, the ζ-potential of the surfactant-free gold nanoparticles in deionized water was −39.94 mV, which implies that the surfaces of AuNPs are negatively charged. As we add formalin to AuNPs solution to make AuNPs:F= 10:1 and AuNPs:F=10:5, the ζ-potential changed to −11.46 mV and +0.30 mV, respectively as listed in Table 2. This manifests that methanediol molecules in formalin work as cationic surfactants in the colloidal solutions and neutralize the surface charges, namely Au-O^- sites of the AuNPs. With increase in the concentration of formalin, the aggregation of AuNPs prevails as shown in Figure 4.

Conclusion

Aggregation of gold nanoparticles mediated by formalin was studied by time-resolved UV-visible spectroscopy, transmission electron microscope (TEM), dynamic light scattering (DLS), and zeta-potential measurements. For three concentration (10:1, 10:5 and 10:7) ratios of AuNPs:F, we observed different types of aggregation and kinetic mechanisms. For 10:1 concentration ratio of AuNPs:F, the main SPR band smoothly decreased, being red-shifted, and a strong secondary SPR band appeared at 725 nm arising from dimer formation. Over time, this dimer band decreased and shifted to red very smoothly due to the evolution to chain structures. After 6 h of incubation time, both SPR bands became very weak due to the formation of network structures from chain structures and, ultimately, global aggregation of AuNPs mediated by formalin. From our DLS measurements, it is apparent that the aggregation of AuNPs is a slow process. For 10:5 ratio, however, the second SPR band was centered at 650 nm while it was at 725 nm for 10:1 ratio. The second SPR band smoothly shifted to red with a strong intensity even after 6 h, which indicates the stability of dimers is pronounced for 10:5 ratio case. On the other hand, aggregation of AuNPs from dimer to network structure was very fast at higher formalin concentration ratio (10:7). To conclude, the average size of AuNPs increased with the increase in formalin concentration due to adsorption of methanediol molecules on the surface of AuNPs via formation of CH-O----Au bond.

Acknowledgments. This research was supported by the Basic Science Research Program through the National Research Foundation of Korea (NRF) funded by the Ministry of Education, Science, and Technology (2012R1A1A2001960).

References

1. Thakor, A. S.; Jokerst, J.; Zavaleta, C.; Massoud, T. F.; Gambhir, S. S. *Nano Lett.* **2011**, *11*, 4029.
2. Ungureanu, C.; Amelink, A.; Rayavarapu, R. G.; Sterenborg, H. J. C. M.; Manohar, S.; Van Leeuwen, T. G. *ACS Nano* **2010**, *4*, 4081.
3. Chen, S. Y.; Mock, J. J.; Hill, R. T.; Chilkoti, A.; Smith, D. R.; Lazarides, A. A. *ACS Nano* **2010**, *4*, 6535.
4. Qian, W.; Murakami, M.; Ichikawa, Y.; Che, Y. *J. Phys. Chem. C* **2011**, *115*, 23293.
5. Park, S.; Yang, P.; Corredor, P.; Weaver, M. J. *J. Am. Chem. Soc.* **2002**, *124*, 2428.
6. Itoh, H.; Naka, K.; Chujo, Y. *J. Am. Chem. Soc.* **2004**, *126*, 3026.
7. Jia, H. Y.; Liu, Y.; Zhang, X. J.; Han, L.; Du, L. B.; Tian, Q.; Xu, Y. C. *J. Am. Chem. Soc.* **2009**, *131*, 40.
8. Brust, M.; Gordillo, G. J. *J. Am. Chem. Soc.* **2012**, *134*, 3318.
9. Toster, J.; Iyer, K. S.; Burtovyy, R.; Burgess, S. S. O.; Luzinov, I. A.; Raston, C. L. *J. Am. Chem. Soc.* **2009**, *131*, 8356.
10. Kang, B.; Mackey, M. A.; El-Sayed, M. A. *J. Am. Chem. Soc.* **2010**, *132*, 1517.
11. Odom, T. W.; Nehl, C. L. *ACS Nano* **2008**, *2*, 612.
12. Daniel, M. C.; Astruc, D. *Chem. Rev.* **2004**, *104*, 293.
13. Ghosh, S. K.; Pal, T. *Chem. Rev.* **2007**, *107*, 4497.
14. Myroshnychenko, V.; Fernandez, J. R.; Santos, I. P.; Funston, A. M.; Novo, C.; Mulvaney, P.; Liz-Marzan, L. M.; Abajo, F. J. G. D. *Chem. Soc. Rev.* **2008**, *37*, 1792.
15. Willets, K. A.; Van Duyne, R. P. *Annu. Rev. Phys. Chem.* **2007**, *58*, 267.
16. Kelly, K. L.; Coronado, E.; Zhao, L. L.; Schatz, G. C. *J. Phys. Chem. B* **2003**, *107*, 668.
17. Li, M.; Cushing, S. K.; Wang, Q.; Shi, X.; Hornak, L. A.; Hong, Z.; Wu, N. *J. Phys. Chem. Lett.* **2011**, *2*, 2125.
18. Singh, M. P.; Strouse, G. F. *J. Am. Chem. Soc.* **2010**, *132*, 9383.
19. Pendry, J. *Science* **2002**, *285*, 1687.
20. Liu, J.; Lu, Y. *J. Am. Chem. Soc.* **2004**, *126*, 12298.
21. Saha, K.; Agasti, S. S.; Kim, C.; Li, X.; Rotello, V. M. *Chem. Rev.* **2012**, *112*, 2739.
22. Kumar, S. S.; Kwak, K.; Lee, D. *Anal. Chem.* **2011**, *83*, 3244.
23. Castillejos, E.; Suarez, E. G.; Baeza, B. B.; Bacsa, R.; Serp, P.; Ruiz, A. G.; Ramos, I. R. *Catal. Commun.* **2012**, *22*, 79.
24. Trammell, S. A.; Nita, R.; Moore, M.; Zabetakis, D.; Chang, E.; Knight, D. A. *Chem. Commun.* **2012**, *48*, 4121.
25. Xiao, F. *J. Mater. Chem.* **2012**, *22*, 7819.
26. Tao, C.; An, Q.; Zhu, W.; Yang, H.; Li, W.; Lin, C.; Xu, D.; Li, G. *Chem. Commun.* **2011**, *47*, 9867.
27. Feng, Y.; Wang, Y.; Wang, H.; Chen, T.; Tay, Y. Y.; Yao, L.; Yan, Q.; Li, S.; Chen, H. *Small* **2012**, *8*, 246.
28. Graham, D. *Angew. Chem. Int. Ed.* **2010**, *49*, 9325.
29. Park, W. H.; Kim, Z. H. *Nano Lett.* **2010**, *10*, 4040.
30. Yang, M.; Puebla, R. A.; Kim, H. S.; Potel, P. A.; Liz-Marzan, L. M.; Kotov, N. A. *Nano Lett.* **2010**, *10*, 4013.
31. Hossain, M. K.; Shimada, T.; Kitajima, M.; Imura, K.; Okamoto, H. *Langmuir* **2008**, *24*, 9241.
32. Zhang, X.; Sun, B.; Friend, R. H.; Guo, H.; Nau, D.; Giessen, H.

Nano Lett. **2006**, *6*, 651.
33. Chandrasekharan, N.; Kamat, P. V. *Nano Lett.* **2001**, *1*, 67.
34. Girard, C.; Dujardin, E.; Li, M.; Mann, S. *Phys. Rev. Lett.* **2006**, *97*, 100801.
35. Waele, R. D.; Koenderink, A. F.; Polman, A. *Nano Lett.* **2007**, *7*, 2004.
36. Harris, N.; Arnold, M. D.; Blaber, M. G.; Ford, M. J. *J. Phys. Chem. C* **2009**, *113*, 2784.
37. Bernard, L.; Kamdzhilov, Y.; Calame, M.; Molen, S. J. V. D.; Liao, J.; Schonenberger, C. *J. Phys. Chem. C* **2007**, *111*, 18445.
38. Aslan, K.; Luhrs, C. C.; Perez-Luna, V. H. *J. Phys. Chem. B* **2004**, *108*, 15631.
39. Storhoff, J. J.; Lazarides, A. A.; Mucic, R. C; Mirkin, C. A.; Letsinger, R. L.; Schatz, G. C. *J. Am. Chem. Soc.* **2000**, *122*, 4640.
40. Si, S.; Mandal, T. K. *Langmuir* **2007**, *23*, 190.
41. Li, D.; He, Q.; Cui, Y.; Li, J. *Chem. Mater.* **2007**, *19*, 412.
42. Zhu, M. Q.; Wang, L. Q.; Exarhos, G. J.; Li, A. D. Q. *J. Am. Chem. Soc.* **2004**, *126*, 2656.
43. Nengsih, S.; Umar, A. A.; Salleh, M. M.; Yahaya, M. *Key Eng. Mater.* **2012**, *495*, 79.
44. Le Botlan, D. J.; Mechin, B. G.; Martin, G. J. *Anal. Chem.* **1983**, *55*, 587.
45. Raja, D. S.; Sultana, B. *J. Environ. Health* **2012**, *74*, 36.
46. Mandin, C.; Dor, F.; Boulanger, G.; Cabanes, P. A.; Solal, C. *Environ. Risque Sante* **2012**, *11*, 27.
47. Shin, H. S.; Lim, H. H. *Int. J. Food Sci. Technol.* **2012**, *47*, 350.
48. Kumari, A.; Lim,Y. X.; Newell, A. H.; Olson, S. B.; McCullough, A. K. *DNA Repair* **2012**, *11*, 236.
49. Nengsih, S.; Umar, A. A.; Salleh, M. M.; Oyama, M. *Sensors* **2012**, *12*, 10309.
50. Lebrun, N.; Dhamelincourt, P.; Focsa, C.; Chazallon, B.; Destombes, J. L.; Prevost, D. *J. Raman Spectrosc.* **2003**, *34*, 459.
51. Mohlmann, G. R. *J. Raman Spectrosc.* **1987**, *18*, 199.
52. Mafune, F.; Kohno, J. Y.; Takeda, Y.; Kondow, T. *J. Phys. Chem. B* **2001**, *105*, 5114.
53. Nichols, W. T.; Sasaki, T.; Koshizaki, N. *J. Appl. Phys.* **2006**, *100*, 114913.
54. Quinten, M.; Kreibig, U. *Surface Sci.* **1986**, *172*, 557.
55. Link, S.; El-Sayed, M. A. *J. Phys. Chem. B* **1999**, *103*, 8410.
56. Mulvaney, P. *Langmuir* **1996**, *12*, 788.
57. Duy, J.; Connell, L. B.; Eck, W.; Collins, S. D.; Smith, R. L. *J. Nanopart. Res.* **2010**, *12*, 2363.
58. Aslan, K.; Perez-Luna, V. H. *Langmuir* **2002**, *18*, 6059.
59. Eck, D.; Helm, C. A.; Wagner, N. J.; Vaynberg, K. A. *Langmuir*, **2001**, *17*, 957.
60. Bohren, C. F.; Huffman, D. R. *Absorption and Scattering of Light by Small Particles*; Wiley: New York, 1983.
61. Mie, G. *Ann. Phys. (Leipzig)* **1908**, *25*, 377.
62. Kreibig, U.; Vollmer, M.; Toennies, J. P. *Optical Properties of Metal Clusters*; Springer-Verlag: Berlin, 1995.
63. Perenboom, J. A. A. J.; Wyder, P.; Meier, F. *Phys. Rep.* **1981**, *78*, 173.
64. Taylor, R. W.; Lee, T. C.; Scherman, O. A.; Esteban, R.; Aizpurua, J.; Huang, F. M.; Baumberg, J. J.; Mahajan, S. *ACS Nano* **2011**, *5*, 3878.
65. Link, S.; El-Sayed, M. A. *J. Phys. Chem. B* **1999**, *103*, 4212.
66. Sharma, D. *Colloids Surf., B* **2011**, *85*, 330.
67. Muto, H.; Yamada, K.; Miyajima, K.; Mafune, F. *J. Phys. Chem. C* **2007**, *111*, 17221.
68. Amendola, V.; Polizzi, S.; Meneghetti, M. *Langmuir* **2007**, *23*, 6766.
69. Amendola, V.; Meneghetti, M. *J. Mater. Chem.* **2007**, *17*, 4705.
70. Amendola, V.; Polizzi, S.; Meneghetti, M. *J. Phys. Chem. B* **2006**, *110*, 7232.
71. Sylvestre, J. P.; Poulin, S.; Kabashin, A. V.; Sacher, E.; Meunier, M.; Luong, J. H. T. *J. Phys. Chem. B* **2004**, *108*, 16864.